Paleoceanography and Paleoclimatology

RESEARCH ARTICLE
10.1029/2020PA004142

Estimating Bioturbation From Replicated Small-Sample Radiocarbon Ages

Andrew M. Dolman[1], Jeroen Groeneveld[1,2], Gesine Mollenhauer[3,4,5], Sze Ling Ho[6], and Thomas Laepple[1,4,5]

[1]Alfred-Wegener-Institut Helmholtz-Zentrum für Polar-und Meeresforschung, Potsdam, Germany, [2]Institute of Geology, Hamburg University, Hamburg, Germany, [3]Alfred-Wegener-Institut Helmholtz-Zentrum für Polar-und Meeresforschung, Bremerhaven, Germany, [4]Department of Geosciences, University of Bremen, Bremen, Germany, [5]MARUM – Center for Marine Environmental Sciences and Faculty of Geosciences, University of Bremen, Bremen, Germany, [6]Institute of Oceanography, National Taiwan University, Taipei, Taiwan

Key Points:

- Age-heterogeneity within sediment layers adds hidden uncertainty to radiocarbon-based age estimates
- The amount of age-heterogeneity depends on the sedimentation rate and bioturbation mixing depth
- We present a method to estimate ^{14}C age-heterogeneity and lookup figure to estimate age uncertainty

Supporting Information:

Supporting Information may be found in the online version of this article.

Correspondence to:

A. M. Dolman,
andrew.dolman@awi.de

Citation:

Dolman, A. M., Groeneveld, J., Mollenhauer, G., Ho, S. L., & Laepple, T. (2021). Estimating bioturbation from replicated small-sample radiocarbon ages. *Paleoceanography and Paleoclimatology*, *36*, e2020PA004142. https://doi.org/10.1029/2020PA004142

Received 6 OCT 2020
Accepted 14 JUN 2021

Abstract Marine sedimentary records are a key archive when reconstructing past climate; however, mixing at the seabed (bioturbation) can strongly influence climate records, especially when sedimentation rates are low. By commingling the climate signal from different time periods, bioturbation both smooths climate records, by damping fast climate variations, and creates noise when measurements are made on samples containing small numbers of individual proxy carriers, such as foraminifera. Bioturbation also influences radiocarbon-based age-depth models, as sample ages may not represent the true ages of the sediment layers from which they were picked. While these effects were first described several decades ago, the advent of ultra-small-sample ^{14}C dating now allows samples containing very small numbers of foraminifera to be measured, thus enabling us to directly measure the age-heterogeneity of sediment for the first time. Here, we use radiocarbon dates measured on replicated samples of 3–30 foraminifera to estimate age-heterogeneity for five marine sediment cores with sedimentation rates ranging from 2 to 30 cm kyr^{-1}. From their age-heterogeneities and sedimentation rates we infer mixing depths of 10–20 cm for our core sites. Our results show that when accounting for age-heterogeneity, the true error of radiocarbon dating can be several times larger than the reported measurement. We present estimates of this uncertainty as a function of sedimentation rate and the number of individuals per radiocarbon date. A better understanding of this uncertainty will help us to optimize radiocarbon measurements, construct age models with appropriate uncertainties and better interpret marine paleo records.

1. Introduction

Proxy records recovered from sediments are an important source of information about the history of the Earth's climate prior to the instrumental era. For example, the ratio of magnesium to calcium (Mg/Ca) in the shells of marine organisms such as foraminifera contains information about the temperature of the environment in which calcification took place (Lea, 2014; Nürnberg et al., 1996; Rosenthal et al., 2000). These shells settle to the sediment surface and are buried as further sediment accumulates. Over time this produces an archive of recorded (proxy) temperatures that can be read in sequence by taking a sediment core and measuring the Mg/Ca ratio of shells found at progressively deeper, and therefore older, positions in the core.

To obtain a down-core proxy record, samples of foraminiferal shells (hereafter foraminifera) are picked from a series of sediment slices or down-core samples. Assuming, for example, that these slices are 1 cm thick and come from a core location with a constant sedimentation rate of 5 cm kyr^{-1}, foraminifera from a single slice would have a uniform distribution of ages with a width of 200 years, with a corresponding standard deviation (SD) of 58 years, which comes from the formula for the standard deviation of a uniform distribution. However, wherever oxygenated, the surface layer of marine and freshwater sediments is mixed or bioturbated by the burrowing and feeding actions of benthic organisms, thus increasing the age-heterogeneity of material at a given depth (Boudreau, 1998; Guinasso & Schink, 1975). For simple models of sediment mixing, the standard deviation of ages at a given depth is simply the ratio of the mixed depth L and the sediment accumulation rate s (Berger & Heath, 1968; Guinasso & Schink, 1975). For a core with a 5 cm kyr^{-1} sedimentation rate and 10 cm bioturbation depth, $L/s = 2000$ years, and therefore bioturbation greatly increases the expected age-heterogeneity of a sediment slice from 58 to approximately 2000 years.

Further to this simple model, changes over time in the abundance of the foraminifera species being dated can compound the effects of bioturbation, creating both temporal offsets (Ausín et al., 2019; Bard et al., 1987; Costa et al., 2018; Löwemark et al., 2008) and changes in age-heterogeneity (Andree, 1987; Lougheed et al., 2020). In sediment horizons corresponding to periods of low abundance, foraminiferal tests will be preferentially mixed in from adjacent periods of high abundance, increasing age-heterogeneity in that horizon. Conversely, during periods of high abundance, proportionally fewer foraminifera are mixed in from adjacent depths, resulting in lower age-heterogeneity. For this reason it is recommended to pick foraminifera for dating and paleo-proxy extraction from horizons with high abundance (Bard et al., 1987).

The additional age-heterogeneity created by bioturbation has important implications for sedimentary proxy records. Proxies measured on samples containing multiple individual signal carriers (e.g., foraminifera) will represent means over the time periods that have been mixed together. This has a smoothing or filtering effect on any signal, so that the observed amplitude of climate variations is reduced (Anderson, 2001; Bard et al., 1987; Goreau, 1980). In addition to this smoothing effect, if proxies are measured on samples containing only a small number of individual signal carriers, the resulting values will be noisy means of the climate state over the time interval that has been mixed together (Dolman et al., 2020; Kunz et al., 2020; Schiffelbein & Hills, 1984). It would therefore be very useful to have an estimate of the degree of age-heterogeneity when interpreting proxy climate records.

Radiocarbon dating is the principle method used to estimate the age of sediment material younger than about 50 ka BP. The age inferred from the measured radiocarbon content is an estimate of the mean ^{14}C age (or calendar age after calibration) of the particles in a given sample, and similarly, the reported machine error represents uncertainty in the age of the specific sample. However, the particles in a given sample are themselves only a sub-sample of the material from a given depth, and there is therefore additional, hidden, uncertainty about how representative the sample is of the age of the rest of the material from the same depth. Traditionally, radiocarbon dating required large samples of material that would necessarily include 100s of individual foraminifera (typically the equivalent of 1–5 mg C). Therefore, although it would give no indication of the heterogeneity in the age of the material, a single radiocarbon date would be a good estimate of the mean age of material at a given depth. However, the advent of ultra-small sample radiocarbon dating means that samples consisting of very small numbers of foraminifera can now be dated (Fagault et al., 2019; Gottschalk et al., 2018; Lougheed et al., 2012; Wacker et al., 2010, 2013). With fewer individuals per sample, radiocarbon measurements become noisier estimates of the mean age of material at a given depth. However, by radiocarbon dating replicated samples of just a few individual foraminifera we can use this "noise" to estimate the age-heterogeneity of the sediment and to aid our interpretation of proxy climate records based on the down-core mean.

As described above, assuming a simple sediment mixing model, age-heterogeneity can be predicted from the ratio of the mixing depth and sedimentation rate, L/s. However, while the sedimentation rate for a given core can be readily determined using a series of down-core radiocarbon dates, the mixing depth is harder to estimate. Direct measurements using particle tracers of the mixing depth at the core-top show that L is highly variable in space ($8.37 + -6.19$ cm, Teal et al., 2010) and mixing intensity may be particle size dependent (Thomson et al., 1995; Wheatcroft, 1992). The life-span of the tracer may also influence mixing depth estimates as short life-span tracers, such as ^{210}Pb (half-life 26 years) may simply miss sporadic mixing events that compound over time to produce the long-term mixing behavior. These direct estimates of mixing depth are rarely available at proxy record core sites and in any-case only provide an estimate of the current mixing depth and cannot inform us about mixing depths in the past when the sediment archive was formed.

The mixing depth at the core-top can also be inferred from the "kink" in a series of down-core ^{14}C measurements (e.g., Peng & Broecker, 1984; Trauth et al., 1997), but this requires a large number of measurements in the first 0–20 cm of the sediment core, and for gravity and piston cores the upper few centimetres are often lost during recovery. Although they integrate mixing over a longer time period than tracer experiments, kink based estimates also cannot tell us about past mixing depths. Tephra layers can be used to infer mixing depths where they occur in the down-core record by fitting the impulse response function of a mixing model to the distribution of the glass shards preserved in the sediment. For example, Bard et al. (1994) estimated mixing depths of 5, 10 and 13 cm based on the distribution of the Vedde Ash layer in three North Atlantic cores; in a fourth core the ash layer was too irregular to fit. In contrast, Thornalley et al. (2010) inferred

Table 1
Sediment Cores Sampled in This Study With Their Locations and the Research Cruise During Which the Core was Taken

Core	Cruise	Latitude	Longitude	Water depth [m]
GeoB 10054-4	SO184	8°40′54″S	112°40′6″E	1,076
GeoB 10066-7	SO184	9°23′33.6″S	118°34′31.8″E	1,635
OR1-1218-C2-BC	OR1-1218	10°54′1.8″N	115°18′27.6″E	2,208
GeoB 10058-1	SO184	8°40′S	112°38′E	1,103
SO213-84-2	SO213/2	45°7′28.2″S	174°35′11.4″E	992

mixing depths of just 2 cm using the Vedde and Katla Ash layers in core RAPiD-15-4P on the South Iceland Rise.

The above methods all estimate the mixing depth, from which a prediction of age-heterogeneity can be made. Here we propose and test a method to directly estimate the age-heterogeneity of sediment by radiocarbon dating replicated samples of small numbers (3–30) of foraminifera and using the age-variation between these samples to estimate inter-individual age-heterogeneity. From these age-heterogeneities we can then infer bioturbation depths, and this can be achieved for any down-core position within the age range for radiocarbon dating. We use a proxy forward model (sedproxy, Dolman & Laepple, 2018) to test for the potential influence of abundance changes on the measured age-heterogeneity and inferred bioturbation depths. The wider use of this method would allow for a more rigorous interpretation of proxy climate records by providing direct estimates of age-heterogeneity and its smoothing effect on a per-core basis. The hidden uncertainty in radiocarbon based age-control points can also be estimated, resulting in better age-depth models. With this knowledge we can also further optimize future drilling campaigns sampling strategies. We examine the necessary conditions to use this method and estimate correction factors for the bias due to the exponential relationship between radiocarbon activity and age.

2. Materials and Methods

2.1. Physical Sampling and Radiocarbon Dating

We used foraminifera picked from five sediment cores recovered that span a range of sediment accumulation rates (approximately 2–30 cm kyr^{-1}). The sites were sampled as part of the SO184, SO213/2 and OR1-1218 cruises (Table 1, Figure 1) (Hebbeln & cruise participants, 2006; Tiedemann et al., 2014). Radiocarbon dating was performed on samples of single species of foraminifera picked from discrete 1 cm thick sediment slices. With the exception of one sample from GeoB 10066-7, a single species was used from each core, either *Globigerina bulloides* (SO213-84-2, 250–400 μm size fraction) or *Trilobatus sacculifer* without sac-like final chamber (GeoB 10054-4, GeoB 10058-1, GeoB 10066-7, 250–400 μm size fraction; and OR1-1218-C2-BC, 300–355 μm or 315–355 μm) (Table 2).

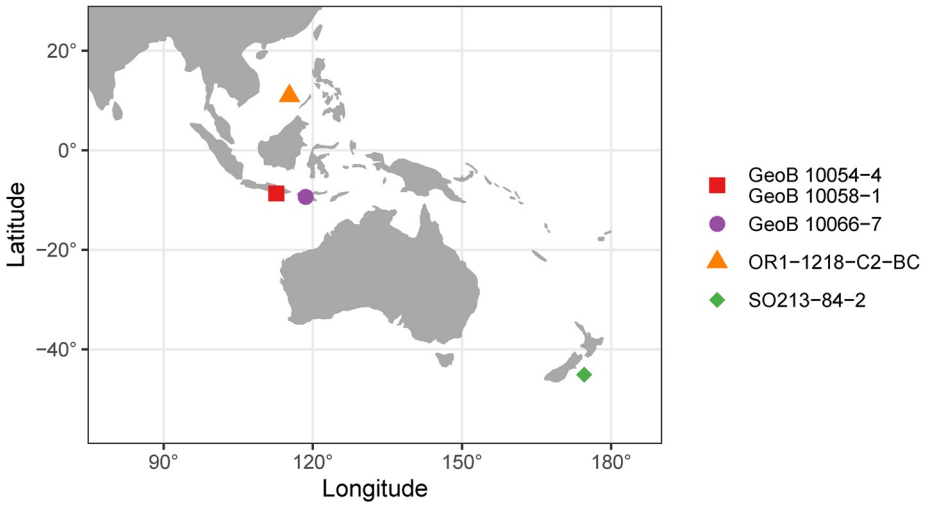

Figure 1. Locations of cores used in this study. Additional data from two cores in the North Atlantic Ocean, T86-10P (Lougheed et al, 2018) (37°8′130 N, 29°59′150 W), and MD08-3178 (Fagault et al, 2019) (31°17.09′ N, 11°29.20′ W) are included in the discussion but the core locations are outside the range of this map and not shown. GeoB 10054-4 and GeoB 10058-1 are a gravity core and multicore respectively, taken at sites approximately 3 km apart.

Table 2
Summary of Radiocarbon Dating per Core and Depth. Sub-Core or Tube is Indicated in Parentheses When Appropriate. n_f is the Number of Individual Foraminifera per Radiocarbon Dated Sample, n_{rep} is the Number of Replicated Radiocarbon Dated Samples

Core	Core depth [cm]	Species	Size fraction [μm]	n_f	n_{rep}
GeoB 10054-4	28–29	*T. sacculifer*	250–400	50	1
GeoB 10054-4	48–49	*T. sacculifer*	250–400	50	1
GeoB 10054-4	68–69	*T. sacculifer*	250–400	10	10
GeoB 10054-4	88–89	*T. sacculifer*	250–400	50	1
GeoB 10058-1	11–12	*T. sacculifer*	250–400	5–6	20
GeoB 10058-1	17–18	*T. sacculifer*	250–400	110	1
GeoB 10058-1	20–21	*T. sacculifer*	250–400	110	1
GeoB 10058-1	23–24	*T. sacculifer*	250–400	110	1
GeoB 10058-1	26–27	*T. sacculifer*	250–400	110	1
GeoB 10058-1	29–30	*T. sacculifer*	250–400	5–6	20
GeoB 10066-7	23–24	*T. sacculifer*	250–400	50	1
GeoB 10066-7	48–49	*T. sacculifer*	250–400	49	1
GeoB 10066-7[a]	53–54	*G. bulloides*	250–400	10	10
GeoB 10066-7	98–99	*T. sacculifer*	250–400	53	1
OR1-1218-C2-BC (1)	36–37	*T. sacculifer*	315–355	5	10
OR1-1218-C2-BC (1)	36–37	*T. sacculifer*	300–355	30	1
OR1-1218-C2-BC (1)	36–37	*T. sacculifer*	315–355	200	3
OR1-1218-C2-BC (7,8,9)	10–12	*T. sacculifer*	315–355	200	6
SO213-84-2 (1)	1–2	*G. bulloides*	250–400	5–6	10
SO213-84-2 (1)	18–19	*G. bulloides*	250–400	>350	1
SO213-84-2 (1)	23–24	*G. bulloides*	250–400	5–6	10
SO213-84-2 (1)	23–24	*G. bulloides*	250–400	>350	1
SO213-84-2 (2)	17–18	*G. bulloides*	250–400	>350	1
SO213-84-2 (2)	20–21	*G. bulloides*	250–400	>350	1
SO213-84-2 (3)	17–18	*G. bulloides*	250–400	>350	1
SO213-84-2 (3)	21–22	*G. bulloides*	250–400	3	12
SO213-84-2 (3)	21–22	*G. bulloides*	250–400	5–6	10
SO213-84-2 (3)	21–22	*G. bulloides*	250–400	30	8
SO213-84-2 (3)	22–23	*G. bulloides*	250–400	>350	1

[a]*G. bulloides* were picked from a single slice from GeoB 10066-7.

To estimate sediment age-heterogeneity, replicated "small-*n*" radiocarbon dates were measured on samples consisting of between three and 30 individual foraminifera, n_f, with multiple replicate samples taken from each sediment slice, n_{rep}. We use the term "small-*n*" to refer specifically to samples consisting of material from a small number of individual foraminifera, regardless of the mass of the sample. Samples with a small mass of carbon could potentially contain parts from a great many individuals if these are first crushed and mixed before sub-sampling. Additional radiocarbon dating was performed on non-replicated "bulk" samples consisting of larger numbers of foraminifera, to provide down-core age control points for estimating sediment accumulation rates. With the exception of the bulk samples from core SO213-84-2, all Accelerated Mass Spectrometry (AMS) ^{14}C dates were generated using a Mini Carbon Dating System (MICADAS) at the Alfred Wegener Institute, Bremerhaven, Germany, following standard operating procedures (Mollenhauer et al., 2021; Wacker et al., 2010). MICADAS' capability of analyzing a gas target was used for small-*n* samples (Ruff et al., 2010), larger samples were measured using a graphite target. Blank correction of foraminifera samples was performed against sample-size matched Eemian-age foraminifera from GeoB 3316-1. Blanks were processed and correction performed according to a procedure in Sun et al. (2020). Radiocarbon dating of the bulk samples from core SO213-84-2 was carried out at NOSAMS, Woods Hole Oceanographic Institution and Keck Carbon Cycle AMS Laboratory, University of California, Irvine.

Radiocarbon dates were converted to calendar ages using the Marine20 calibration (Heaton et al., 2020) and the *R* package Bchron (Haslett & Parnell, 2008). The Marine20 calibration includes a time-varying global marine reservoir effect (ΔR). We did not adjust for local marine reservoir effects and assumed no uncertainty in ΔR. High frequency changes in the local reservoir age could potentially increase the variation in radiocarbon age measured in a given sediment slice, which would inflate the inferred age-heterogeneity, we omit this effect here. For each sample, the probability density function (PDF) for calendar age was summarized by its median and standard deviation, as none of the PDFs were bi- or multi-modal. Multi-modality may be more of a concern when using the Intcal20 calibration curve for terrestrial samples, as smoothing of the cosmogenic radiocarbon signal in the atmosphere is much less than that in the ocean (Bard & Heaton, 2021).

Sediment accumulation rates were estimated by linear regression of calibrated calendar age on depth. Bulk and small-*n* dates from the depth range 15–100 cm (10–37 cm for OR1-1218-C2-BC) were used so as to exclude the mixed layer and to estimate the sediment accumulation rate over the range of depths for which replicated ^{14}C measurements were made. For replicated small-*n* dates, a mean date was first calculated for each depth. The multicore GeoB 10058-1 and gravity core GeoB 10054-4 were intended to be taken at the same site, but due to technical difficulties were in fact taken on subsequent days at locations 3 km apart (Hebbeln & cruise participants, 2006). However, their down-core radiocarbon data indicate very similar sedimentation rates (approximately 16 cm kyr^{-1}) and we combined these to create a single more robust sedimentation rate estimate.

2.2. Estimation of Age-Heterogeneity

For each sediment slice, we calculated the variance between replicated calendar age estimates, σ^2_{rep}. From this we subtracted the mean calendar age uncertainty for samples from that slice, σ^2_{meas}. The calendar age uncertainties are calculated as the standard deviations of the empirical PDFs from the calibration procedure and as such contain the measurement error reported by the MICADAS lab combined with the uncertainty in the calibration, which will be larger in flatter and older parts of the calibration curve. If this variance due to measurement uncertainty is not removed, it will bias estimates of true age-heterogeneity. As the ages of the individuals are independent, the variance between individuals, σ^2_{ind}, can be inferred as the variance between replicates of size n_f multiplied by n_f.

$$\sigma^2_{ind} = n_f\left(\sigma^2_{rep} - \sigma^2_{meas}\right) \tag{1}$$

The inter-individual variance contains a component from the finite sediment width τ_{slice} (here 1 cm) and additional variation due to sediment mixing. We can estimate the variance due to the slice thickness using Equation 2, where the 1/12 comes from the formula for the variance of a uniform distribution. After subtracting the variance due to the slice thickness we attribute the remaining excess variance to bioturbation, assuming that variation in radiocarbon age for cohorts of these mono-specific foraminifera was minimal.

$$\sigma^2_{slice} = \frac{1}{12}\left(1000 \cdot \frac{\tau_{slice}}{s}\frac{[\text{cm}]}{[\text{cm kyr}^{-1}]}\right)^2 \tag{2}$$

$$\sigma^2_{bioturbation} = \sigma^2_{ind} - \sigma^2_{slice} \tag{3}$$

To interpret this value, we use the simple bioturbation model proposed by Berger and Heath (1968) to infer a mixing depth from $\sigma^2_{bioturbation}$. Assuming that the upper L centimetres of sediment are fully and instantaneously mixed but below this level there is no further mixing, and in which the sedimentation rate and flux of foraminifera is assumed to be constant (Berger & Heath, 1968; Matisoff, 1982; Officer & Lynch, 1983), the bioturbation depth required to produce this excess age-variance is given by:

$$L = \frac{s}{1000}\sqrt{\sigma^2_{bioturbation}} \tag{4}$$

2.3. Bias Correction

Due to the exponential relationship between age and radiocarbon activity, estimates of both mean ^{14}C age, and age-variance between multiple samples, are biased because younger individual particles contribute exponentially more to the mean $^{14}C/^{12}C$ ratio. When the underlying age distribution is exponential, and there are infinitely many particles in the sample, there is an analytical formula for the bias in the mean radiocarbon age (Andree, 1987), however, we are not aware of a general solution for finite sample sizes. To address this we carried out a Monte Carlo simulation study to investigate the properties of this bias and to obtain correction factors to adjust our measured age-heterogeneity estimates.

We simulated the process of sampling foraminifera from discrete depths by sampling replicated sets of n_f foraminifera from an exponential age distribution with a standard deviation corresponding to a given combination of L and s. For the purpose of the simulation we ignored the difference between calendar and radiocarbon age and convert the age of each foraminifera to an $F^{14}C$ value with the expression $F^{14}C = e^{\frac{age}{-8033}}$. For each replicate of n_f foraminifera we then calculated its age and mean $F^{14}C$ value. Mean $F^{14}C$ values were then back-transformed to (radiocarbon) ages, $age_{F^{14}C}$. The standard deviation between mean age and mean $age_{F^{14}C}$ values were then calculated for the replicated groups. We repeated this process for a range of underlying age variances and for groups with differing number of foraminifera per $F^{14}C$ "measurement". The

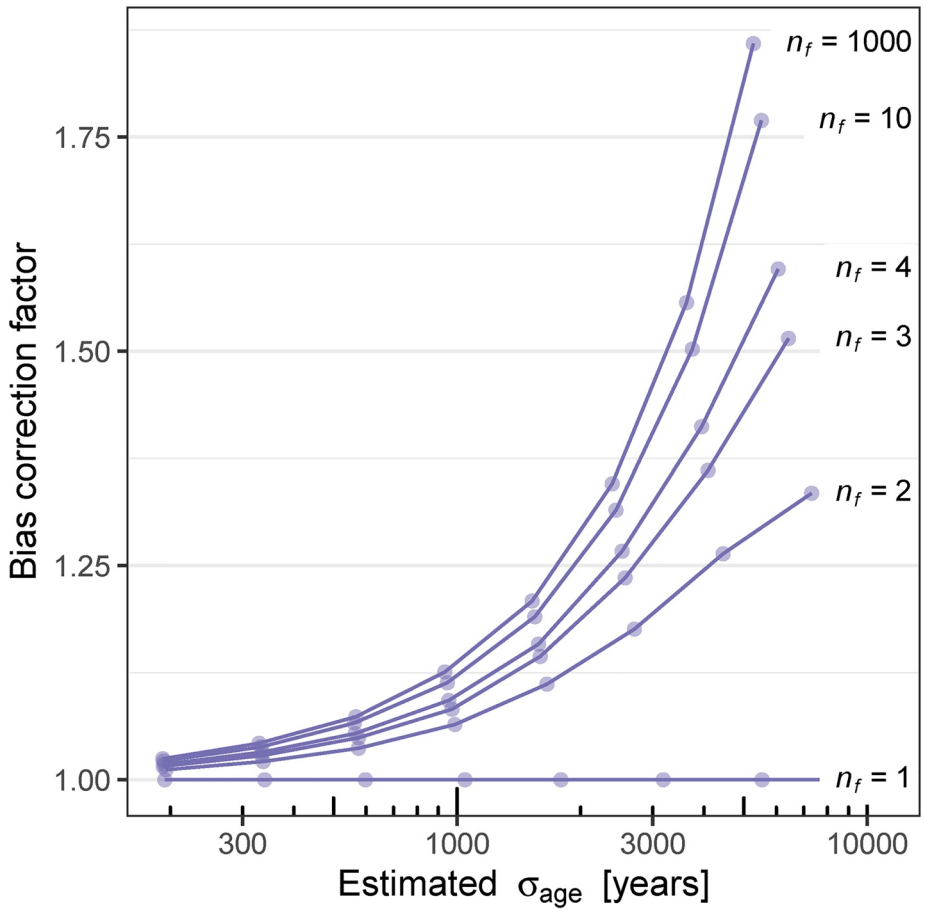

Figure 2. Bias correction factors to correct for the underestimation of age-heterogeneity due to the exponential relationship between radiocarbon activity and age.

difference between the standard deviation in age and standard deviation in $age_{F^{14}C}$ represents the expected bias in estimates of age-heterogeneity.

To adjust for this underestimation of age-heterogeneity we calculated correction factors by which to multiply biased estimates of age-heterogeneity (Figure 2). These correction factors likely represent an upper limit on the potential bias, as the bias depends on the shape of the underlying age distribution. If the true age-distribution differs from the assumed exponential, it is probably less skewed than an exponential and hence would produce a smaller bias. In the results we present both adjusted and un-adjusted age-heterogeneities and implied bioturbation depths. The simulation was written in *R* code and carried out with *R* version 3.6.2 (R Core Team, 2019). For more detail see Supporting Text S1 and Figure S1.

2.4. Modeling the Joint Effect of Bioturbation and Abundance Changes

To assess whether abundance changes in the measured foraminifera may have influenced the age-heterogeneity measured in these cores, we used the proxy forward model sedproxy (Dolman & Laepple, 2018) to simulate small-*n* radiocarbon measurements under scenarios with constant or varying foraminiferal abundance. As the input signal, we used the Marine20 calibration curve, extended back beyond 50 ka BP to 100 ka BP by adding 1 year of radiocarbon age for each calendar year and converted to units of $F^{14}C$. Abundance changes were included as sampling weights via the habitat weights. We compared abundance scenarios of constant foraminifera abundance, an abrupt 10-fold decrease in abundance from Glacial to Holocene at 11.5 ka BP, and a 10-fold increase at 11.5 ka BP, all with a bioturbation depth of 10 cm. Additionally we repeated the constant abundance scenario with a bioturbation depth of 15 cm. The number of individual

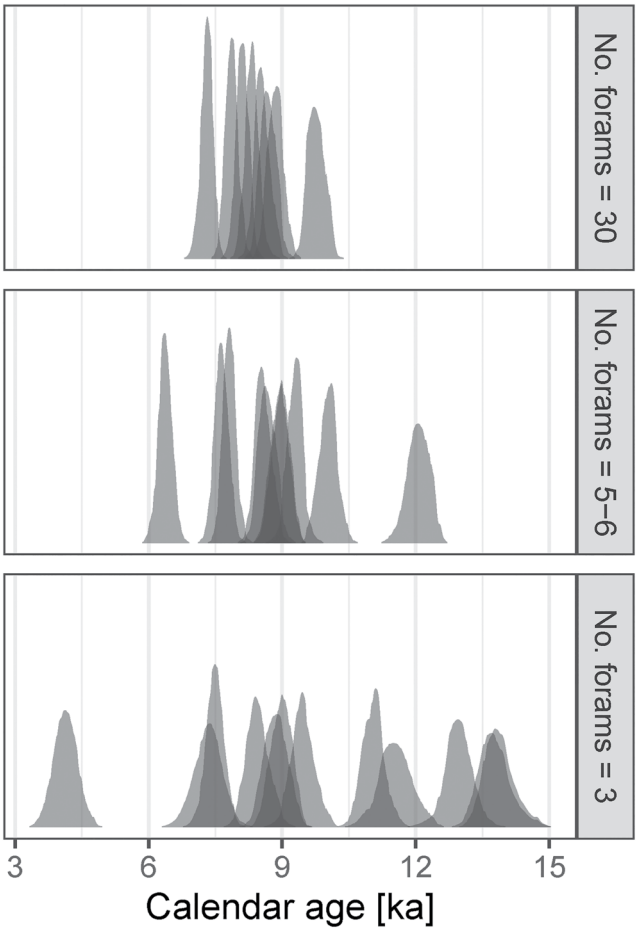

Figure 3. Replicated radiocarbon dates converted to calendar ages from a single 1 cm thick sediment slice, taken at a depth of 21–22 cm, from core SO213-84-2. Each individual density plot shows the probability density function of calendar age obtained by calibrating a radiocarbon age measured on a sample consisting of 3, 5–6 or 30 individual foraminifera (^{14}C age + −1 SD) with the Marine20 calibration curve (Heaton et al., 2020). No local adjustment was made to the global marine reservoir effect contained in Marine20 and we assume no uncertainty in ΔR.

foraminifera per ^{14}C measurement, and number of replicate samples measured at each depth, used in the simulations were all identical to those in the real measurements. We used sedimentation rates estimated from the real data. Each scenario was simulated 1000 times.

3. Results

3.1. Age-Heterogeneity in Core SO213-84-2

We first examine radiocarbon dates from the multicore SO213-84-2, for which we made measurements on groups of 3, 6 and 30 individual foraminifera, all picked from a single depth of multicore tube three (21–22 cm). For samples of 30 individuals, calendar ages range from 7.31 to 9.76 ka BP, with a standard deviation (σ_{rep}) of 726 years, a value far greater than the reported measurement error of about 150 years. Variation in age between samples is even greater for replicates of six foraminifera (range = 6.37–12.07 ka BP, σ_{rep} = 1,521 years) and three foraminifera (range = 4.13–13.85 years BP, σ_{rep} = 2,917 years). Clearly, the calibrated calendar ages of these replicated samples do not agree with each other within their reported uncertainties and this excess variation decreases strongly with the number of foraminifera per measurement (Figure 3). Additional measurements on replicated samples of 5–6 individuals taken from multicore tube one at depths of 1–2 and 23–24 cm have similarly large σ_{rep} values of 1,118 and 1,604 years.

The relationship between σ_{rep} and the number of individuals per measurement very closely follows an inverse relationship (Figure 4). This is a strong indication that inter-individual age variation (σ_{ind}) is the major component of the between sample variation and allows us to infer σ_{ind} by scaling for the number of foraminifera per sample, after first subtracting the much smaller reported measurement error (Equation 1). Inferred age-heterogeneity between individuals, σ_{ind}, from core SO213-84-2 ranges from 2853 to 5027 years (Table 3). Bias correction factors for SO213-84-2 estimated by simulation vary between 1.36 and 1.51, depending on the number of foraminifera per sample. Adjusting for the bias, the range of $\sigma^2_{ind_{adj}}$ increases to 3881–6898 years. Also shown in Table 3 is the much smaller age-heterogeneity of approximately 100 years expected due to the 1 cm thickness of the slice and the 2.9 cm kyr^{-1} sedimentation rate. After subtracting this, and assuming a simple sediment mixing model (Berger & Heath, 1968), the excess age-heterogeneity implies a mixing depth of 11.3–20.0 cm (8.3–14.6 before bias adjustment) (Equations 1–4, Table 3). Age-heterogeneity is somewhat lower for the samples from 1-2 cm deep, which would be in the active mixing layer, than for the other deeper samples.

3.2. Age-Heterogeneity Across Multiple Cores

To test the generality of this result we performed similar replicated small-*n* radiocarbon measurements at four additional sites with sediment accumulation rates of approximately 2, 16 (2 sites), and 29 cm kyr^{-1}. We again adjust the measured age-heterogeneity for bias assuming an exponential age distribution and present both adjusted and un-adjusted age-heterogeneities and bioturbation depths for comparison. To examine the relationship between age-heterogeneity and sedimentation rate across cores, we additionally present the inter-individual age-heterogeneities and implied bioturbation depths for two cores from the Atlantic: core T86-10P published in Lougheed et al. (2018), and core MD08-3178 published in Fagault et al. (2019).

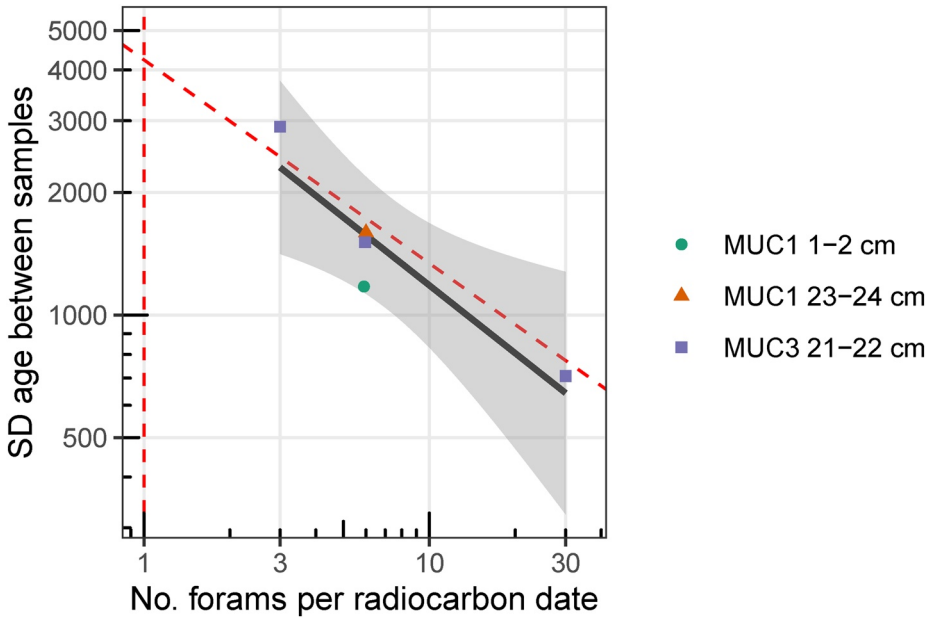

Figure 4. Standard deviation in age between radiocarbon dated samples from core SO213-84-2 as a function of the number of foraminifera they contain. The dashed red lines show extrapolation back to samples of single individual foraminifera assuming the theoretical proportional relationship between standard deviation and the square root of sample size. The samples came from two different multicore tubes of the same deployment.

Estimated age-heterogeneity is again much higher than the measurement error in most cases, with between replicate standard deviations of 281, 594 and 3,130 years, compared to measurement errors of 165, 108, and 301 years (Table 3). The one exception is core GeoB 10066-7 for which σ_{rep} is only 181 years (+−40 SE) compared to a measurement error of 194 years. While this could imply no mixing at all ($L = 0$ cm), because this core has a relatively high sedimentation rate of 29 cm kyr^{-1}, and because the value of σ_{meas} is itself an estimate with its own uncertainty, it is also consistent with mixing of several centi-

Table 3
Measured Standard Deviation Between Replicated ^{14}C Measurements on Small-n Samples of Foraminifera, Inferred Age-Heterogeneity Between Individual Foraminifera and the Implied Bioturbation Depth

Core	Depth [cm]	n_f	n_{rep}	σ_{rep}	$SE_{\sigma_{rep}}$	σ_{meas}	σ_{ind}	Bias	$\sigma_{ind_{adj}}$	σ_{slice}	s	L	L_{adj}
GeoB 10054-4	68.0	10	10	281	54	165	721	1.07	771	17	16.6	11.9	12.8
GeoB 10058-1	11.5	5–6	20	..	..	108	..	1.10	..	17	16.6	..	..
GeoB 10058-1	29.5	5–6	20	594	95	121	1,300	1.10	1,429	17	16.6	21.5	23.7
GeoB 10066-7	53.0	10	10	181	42	[a]194	556	1.05	585	10	29.1	[a]16.2	[a]17.0
OR1-1218-C2-BC	36.5	5	10	3,130	744	301	6,966	1.66	11,563	178	1.6	11.3	18.7
SO213-84-2	1.5	5–6	10	1,188	280	179	2,853	1.36	3,881	99	2.9	8.3	11.3
SO213-84-2	23.5	5–6	10	1,604	381	177	3,905	1.36	5,311	99	2.9	11.3	15.4
SO213-84-2	21.5	3	12	2,917	625	287	5,027	1.37	6,898	99	2.9	14.6	20.0
SO213-84-2	21.5	5–6	10	1,521	360	186	3,682	1.36	5,009	99	2.9	10.7	14.5
SO213-84-2	21.5	30	8	726	192	161	3,879	1.51	5,844	99	2.9	11.3	17.0

Note. n_f is the number of individual formaminifera per radiocarbon measurement, n_{rep} is the number of replicate radiocarbon measurements made on samples of n_f individuals, σ_{rep} is the standard deviation between replicated radiocarbon measurements made from samples from the same sediment slice, $SE_{\sigma_{rep}}$ is the standard error of the estimate of σ_{rep}, σ_{meas} is the reported measurement error, σ_{ind} is the inferred standard deviation in age between individuals.

[a]For GeoB 10066-7, the reported measurement error σmeas was larger than the standard deviation between replicated measurement σrep. To get an upper bound on the possible bioturbation depth we subtracted the error due to binomial counting statistics (see methods).

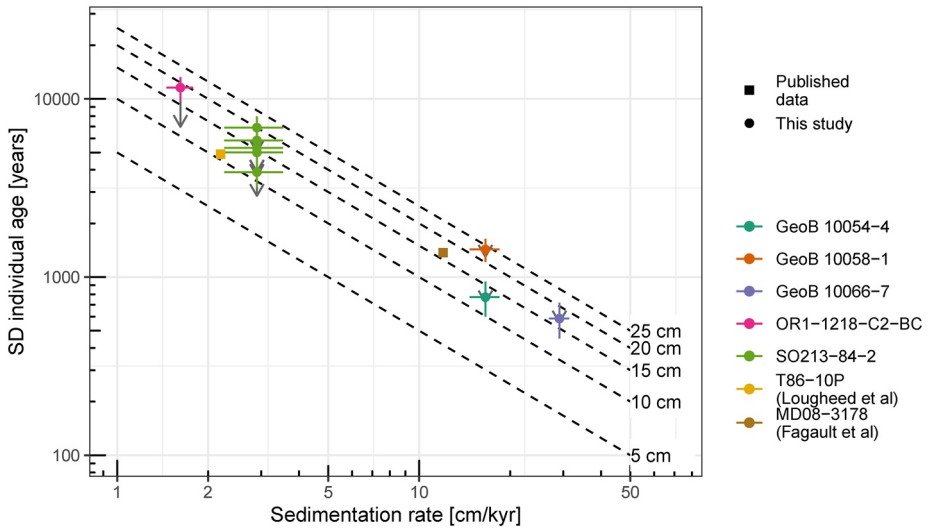

Figure 5. Inferred standard deviation in age between individuals $\sigma_{ind_{adj}}$ plotted against sediment accumulation rate s. Error bars indicate one standard error of the standard deviation and sedimentation rate estimates. The dashed isolines indicate bioturbation depths L consistent with a given sedimentation rate and σ_{ind}. The gray arrows indicate σ_{ind} prior to correcting for the bias due to the exponential relationship between age and radiocarbon content. The bias adjustment is much larger for cores with low sedimentation rates and high estimates of σ_{age}.

metres. For example, assuming a 15 cm bioturbation depth and given the 10 foraminifera per sample, the expected σ_{rep} would be just 164 years. To provide an upper estimate on the inter-individual age-variance and bioturbation depth for this core, we subtract only the error due to the binomial counting statistics for $^{14}C/^{12}C$ (45 years), essentially assigning all additional error to age-heterogeneity. Additionally, several samples taken from GeoB 10058-1 at 11.5 cm deep could not be calibrated with Marine20 as they were younger than the minimum 603 radiocarbon years that can be calibrated with Marine20, including some with negative radiocarbon dates indicating the presence of modern material down to at least 11–12 cm.

Table 4
Sediment Accumulation Rate s (cm kyr^{-1}) and Estimated Bioturbation Depth L (cm) at 4 Sites Measured in This Study, Plus Two Previously Published by Lougheed et al. (2018) Core T86-10p, and Fagault et al. (2019) Core MD08-3178

Core/Site	s	SE$_s$	L	L_{adj}
GeoB 10054-4/58-1	16.6	1.9	15.9	17.3
GeoB 10066-7	29.1	2.3	16.2	17.0
OR1-1218-C2-BC	1.6	0.2	11.3	18.7
SO213-84-2	2.9	0.6	11.2	15.6
MD08-3178	12.0	..	16.5	16.5
T86-10P	2.2	..	10.8	10.8

Note. Estimates for T86-10P and MD08-3178 are based on uncalibrated radiocarbon dates. For MD08-3178, some excess age-heterogeneity may be explained by the sensitive blank correction for these very small samples masses. SEs is the standard error of the estimate of s, Ladj is the inferred bioturbation depth adjusted for the bias due to the exponential relationship between age and radiocarbon content. For GeoB 10066-7 L and Ladj represent upper bounds as we used the error due to binomial counting statistics in place of σmeas (see methods).

Across all analyzed cores we found a strong negative relationship between sedimentation rate s and inter-individual age-heterogeneity, a clear indication that sediment mixing influences age-heterogeneity. Due to this negative relationship, the implied bioturbation depths for all sets of replicated samples fall within a relatively narrow range of 11.3–23.7 cm (Figure 5, Table 3). At the site level, after combining estimates for the same core taken from different depth layers, and combining GeoB 10054-4 and GeoB 10058-1 which come from two sites less than 3 km apart, implied bioturbation depths for the individual sites range from 15.6–18.7 cm (Table 4). For cores T86-10P and MD08-3178 Lougheed et al. (2018) and Fagault et al. (2019) report age-heterogeneities consistent with mixing depths of 10.8 and 19.2 cm, respectively.

The relationship between s and σ_{ind} is only slightly altered by the bias adjustment, which is small compared to other sources of variation in age-heterogeneity. Adjustment is largest for core OR1-1218-C2-BC, for which the simulation study indicated a factor of 1.66, and which has the lowest sedimentation rate and highest estimates of individual age-heterogeneity. The adjustment shifts the implied bioturbation depth from 11.3 to 18.7 cm.

4. Discussion

We found variation in radiocarbon ages between replicated small-*n* samples of foraminifera that far exceeded the reported machine uncertainty at three of the four sites we examined. Between-replicate age-variation was only within the machine uncertainty for core GeoB 10066-7, which has a comparatively high sedimentation rate of 29 cm kyr^{-1}. Age-heterogeneity also far exceeds measurement error for previously published data from two additional cores (Fagault et al., 2019; Lougheed et al., 2018). This excess age-variation can be interpreted as within-sediment-layer heterogeneity caused by bioturbation. Assuming the classical Berger and Heath (1968) mixing model, the implied mixing at the six sites is 11–19 cm. This is somewhat higher than the 10 cm often assumed as a typical value in literature (Boudreau, 1998) and considerably higher than the bioturbation assumed in the interpretation of most paleoclimate records.

Changes over time in the abundance of the measured foraminifer could potentially be increasing the age-heterogeneity in these cores and therefore inflating our estimates of bioturbation depth, as they rely on assuming a constant flux of foraminifera to the sediment. However, for SO213-84-2 we have down-core counts at six depths between 2 and 22 cm. *G. bulloides* was the dominant taxon at all depths, with between 40% and 48% of the total foraminifer composition. While we did not fully quantify down-core foraminiferal abundance for cores GeoB 10054-4/58-1 and GeoB 10066-7, many *T. sacculifer* tests (more than 100 per depth horizon) were picked for additional down-core $\delta^{18}O$ analyses not included here, without a noticeable change in the effort required. For OR1-1218-C2-BC, more than 200 *T. sacculifer* are present in each 1.8 cm^3 down-core sample of sediment. These high densities of foraminifera, without large changes in sediment accumulation rate, preclude very large changes in absolute abundance.

Additionally, our forward modeling simulations indicated that only those measurements from core SO213-84-2 would be susceptible to a glacial to Holocene change in abundance of the measured foraminifer (Figure 6). Other cores were unaffected either because the samples were too deep to be affected (OR1-1218-C2-BC), or too shallow given the sedimentation rate. While, we cannot exclude all possible abundance change scenarios that might have inflated our bioturbation depth estimates, a very particular pattern of abundance change would be required to account for all the sites and depths at which we found high mixing depths. A scenario with constant abundance and a bioturbation depth of 15 cm produced simulated age-heterogeneity that was consistent with all the measured data (Figure 6d).

In principle, $\Delta^{14}C$ variations across the water column also cause some apparent age-heterogeneity due to differences in the calcification depth of the individual foraminifera. However, even assuming a strong $\Delta^{14}C$ gradient (0.2 permille change per meter) and a highly variable calcification depth (uniform probability of calcifying between 0 and 100 m), the resulting heterogeneity ($\sigma = 50$ years) is small compared to the age-heterogeneity found in this study. Over most of the ocean the $\Delta^{14}C$ gradient is weaker than this (Key, 2001), and individual foraminifera may incorporate carbon over a range of depths during their calcification.

The dissolution and fragmentation of foraminiferal tests while they are in the mixed layer can lead to a bias in the ages of surviving tests, as those that reside in the mixed layer longer are more likely to fragment and be lost from the sampled population. The size of this effect varies between taxa according to their susceptibility to dissolution, leading to age-offsets between different species, "the Barker effect" (Barker et al., 2007; Broecker & Clark, 2011). As we analyzed species that are prone to dissolution (Berger, 1968) it is possible that this effect could have biased the mean ages of our samples. However, while this effect would inflate age-heterogeneity for samples of different species, it would have the opposite effect for samples of the same species as used here. Any effect on age-heterogeneity estimates in this study should small due to the location of the cores above the lysocline.

Age-heterogeneity of this magnitude, regardless of the mechanism, has important implications for proxy records recovered from these cores. The climate signal is strongly smoothed by the mixing together of time periods, reducing the inferred amplitude of climate variations (e.g., Anderson, 2001; Schiffelbein, 1985), but, if the proxy measurements are made on small numbers of foraminifera, records can also become noisier as the signal from different climate states is mixed together (Boyle, 1984). In extreme cases measurements can include both glacial and interglacial material. This noise is especially problematic when the variance itself is of interest, for example in individual foraminiferal analyses (Groeneveld et al., 2019; Koutavas & Joanides, 2012; Thirumalai et al., 2013, 2019; Wit et al., 2013). Estimates of age-heterogeneity from replicated

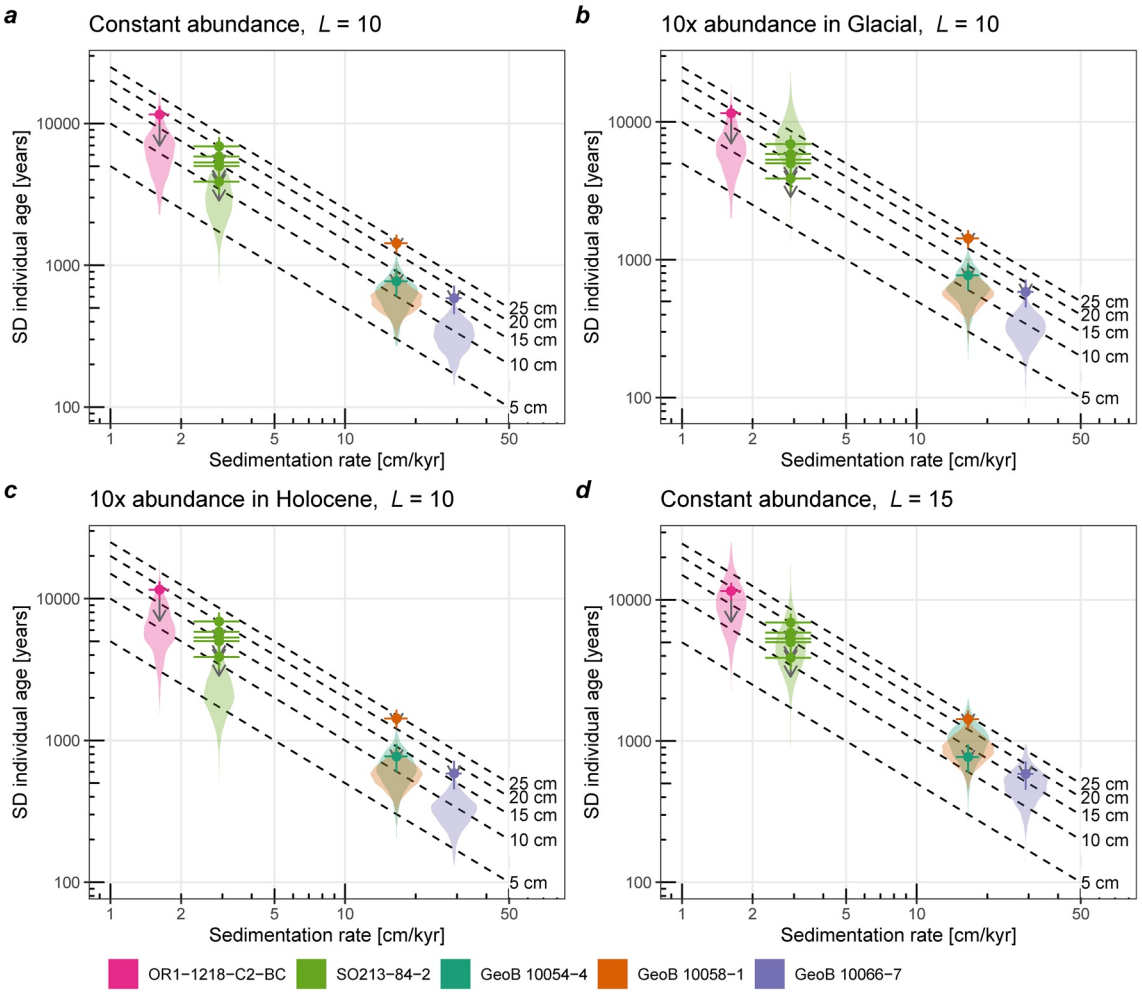

Figure 6. A comparison of measured age-heterogeneity and age-heterogeneity from simulations with abundance changes in the foraminifer. Each sub-figure a-d, shows that same measured data as for Figure 5. The shaded areas behind the measured data points indicate the results from 1,000 replications of a forward model simulation. Panels a, b, and c show the results for simulations with a bioturbation depth of 10 cm; (a) constant abundance, (b) an abrupt 10-fold decline in abundance between the glacial and Holocene at 11.5 ka BP; (c) an abrupt 10-fold increase in abundance between the glacial and Holocene at 11.5 ka BP. Panel d shows results for a constant abundance scenario with a 15 cm bioturbation depth.

small-*n* radiocarbon dates can be used to parametrize proxy forward models to quantitatively assess this smoothing and noise generation (Bard et al., 1987; Dolman & Laepple, 2018; Lougheed, 2020).

A further implication is that radiocarbon dates used for age-depth modeling may require much larger uncertainties than the reported machine errors that are typically used. Although they may correctly quantify the uncertainty in the age of the sample, they ignore the uncertainty in how representative the sample may be of the mean age of material at the depth from which it was recovered (Heegaard et al., 2005). The size of this effect will depend on the bioturbation depth, the sedimentation rate and the sample size. We can see this effect for the low sedimentation rate multicore SO213-84-2, for which a series of down-core radiocarbon dates were made in each of three sub-cores. These replicated age-depth series show very little overlap within their reported age-uncertainties (Figure 7a), despite having been measured on samples of approximately 350 foraminifera each. However, adding the expected uncertainty due to age-heterogeneity brings the three down-core age-depth series into much closer agreement (Figure 7b). Radiocarbon dating small-*n* samples, either because the sediment material contains only few foraminifera or to save picking and processing time, risks further inflating this additional error. To guide the choice of sample size, we have created lookup figures, based on Equation 5, for mixing depths of 5, 10, 15 and 20 cm (Figures 8 and S2) - extending the figure of Andree (1987) into the range of modern small-*n* samples. These can be used to get a rapid idea

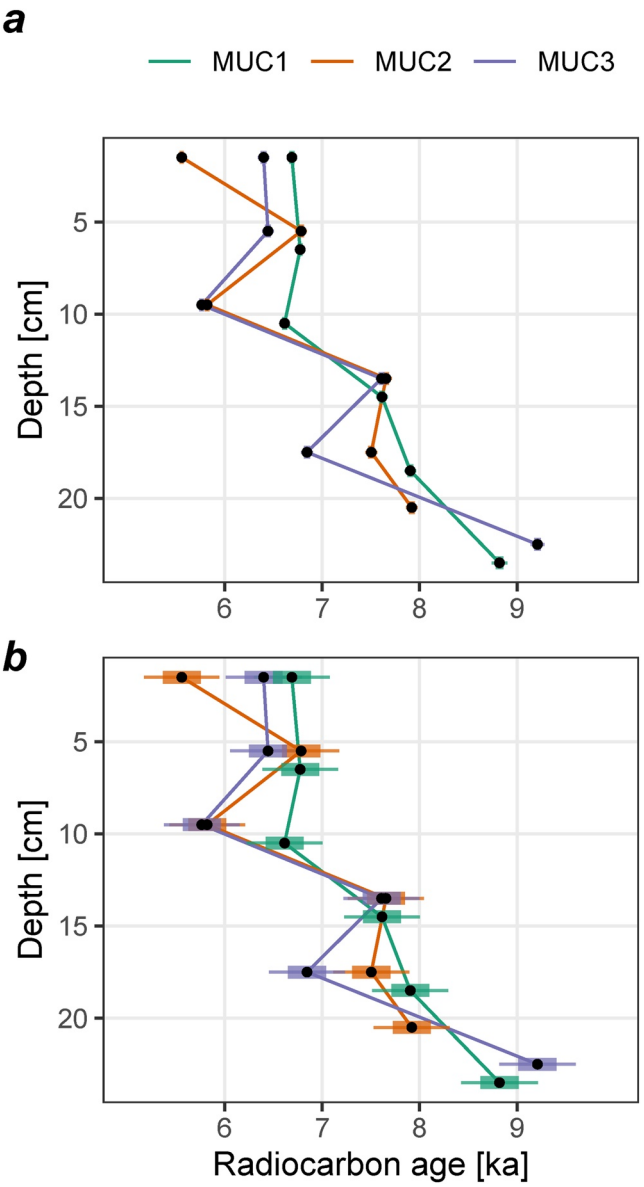

Figure 7. Replicated down-core radiocarbon age estimates for SO213-84-2. Each down-core record corresponds to a separate multicore tube or half tube from the same deployment. Age-uncertainties in subplot (a) indicate σ_{meas}, whereas those in (b) include the inferred σ_{age} between individuals, scaled for samples of 350 individuals. Thick lines indicate 1σ intervals, thin lines are 2σ intervals.

of the number of individual foraminifera per sample required to reduce the additional age-uncertainty below a desired level, or inversely, given a radiocarbon date we can estimate the additional hidden uncertainty from age-heterogeneity from the sedimentation rate and an estimate of the number of individuals in the sample.

$$n_f = \left(\frac{1000L}{s \cdot \sigma_{rep}}\right)^2 \quad (5)$$

4.1. The Physical Mixing Process and Outliers

The concept of a bioturbation depth is an obvious simplification; however, as the age-heterogeneity is related to the sedimentation rate regardless of the precise mixing process (Matisoff, 1982), the specific mixing model assumed is not particularly important for the main conclusions here. We can still however question the extent to which our measured radiocarbon dates are consistent with the Berger and Heath (1968) mixing model. In contrast to Lougheed et al. (2018), who estimated that around 10% of their foraminifera had ages inconsistent with a simple mixing model, we found very few extreme outlying dates which might be evidence of unusually deep mixing events like *Zoophycos* burrows (Küssner et al., 2018; Löwemark & Grootes, 2004; Löwemark & Werner, 2001). However, as we dated samples containing multiple foraminifera, individuals with aberrant ages may be hidden, as every distribution will converge toward a Gaussian distribution as the number of individuals increases (Figure S3). Therefore it is unclear the extent to which additional disturbance by *Zoophycos*, or other deep mixing mechanisms, contribute to the age-heterogeneity we measure. The single clear outlier we did obtain was measured on just three individuals, and was too young by about 5000 years in a core with sedimentation rate of 2.9 cm kyr^{-1} (core SO213-84-2). This implies a relative displacement of approximately 43.5 cm for one of the three foraminifera, which would be consistent with the known size of *Zoophycos* burrows (Wetzel & Werner, 1980). Additional displaced individuals hidden inside multi-individual measurements would mean that we have overestimated the depth of the well mixed layer.

The specific form of mixing and its resulting probability distribution of ages does have implications for the bias generated by the exponential relationship between age and the $^{14}C/^{12}C$ ratio. We calculated biases for the highly skewed exponential distribution resulting from the Berger and Heath (1968) mixing model; less skewed distributions, resulting for example from incomplete mixing or a smooth transition between the mixed layer and the unmixed sediment, will generate a smaller bias. Therefore our bias correction which assumes an exponential distribution may be too strong and probably represents an upper limit. This bias could potentially be eliminated by dating individual foraminifera (e.g., Fagault et al., 2019; Lougheed et al., 2018), which would also remove the issue of hidden outliers.

4.2. Practical Considerations When Applying This Method

We have demonstrated the use of small-*n* radiocarbon measurements to estimate site and core-depth specific age-heterogeneity and infer bioturbational mixing depths. This knowledge is especially important when a high-resolution analysis or the analysis of individual foraminifera (IFA) is planned, and it is our hope that bioturbation estimates will become routine in these applications. However, there are some practical considerations when applying this method.

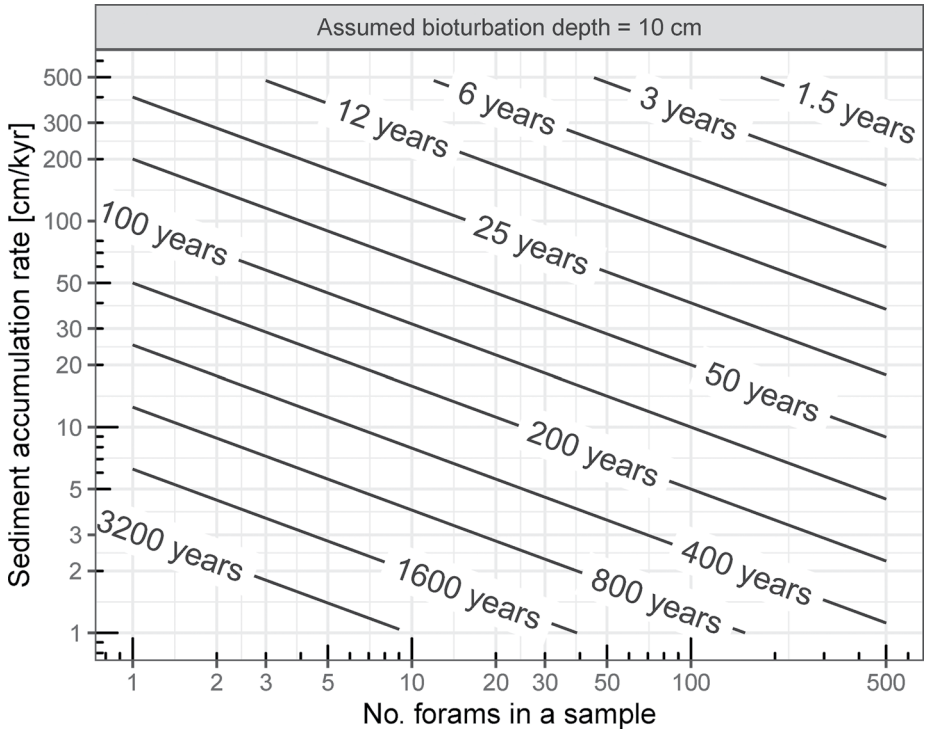

Figure 8. A reference chart to obtain estimates of the additional age-uncertainty σ_{age} for a sample measured on a given number of foraminifera, from the sedimentation rate of the core s, and assuming a bioturbation depth L of 10 cm. Or alternatively, an estimate of the number of foraminifera per sample needed to reduce σ_{age} below a given level. For example, for a core with $s = 5$ cm kyr^{-1}, to get the additional age-uncertainty below 200 years you need at least 100 foraminifera; if s were 20 cm kyr^{-1} you would need only 6–7 foraminifera. The σ_{age} values of the isolines are proportional to L, so if a larger, 20 cm, bioturbation depth is suspected, double the isoline values. Note however, altering the mass of material processed and measured may also influence the reported instrument error - and the characteristic sizes of different foraminiferal taxa will impose their own constraints on the number of specimens required.

First, the estimation only works if the age-heterogeneity is larger than the measurement error. For the data presented here, measurement error ranged from about 80 to 400 years. At sedimentation rates below about 2 cm kyr^{-1}, age-heterogeneity from bioturbation will far exceed this measurement error, even for relatively small bioturbation depths. However, as s rises, the expected age-heterogeneity between individuals (Figure 5, dashed lines), or samples (Figure 8, contour lines), falls rapidly. Furthermore, for many foraminifera taxa, single specimens cannot be dated, even with MICADAS, and so the approach of dating small-n samples has to be used - reducing the signal of age-heterogeneity by a factor of n_f.

Second, the uncertainty, or standard error (SE), of a standard deviation depends on the number of samples measured (Equation 6), hence a sufficient number of small-n samples needs to be measured in order to get a reliable estimate of σ_{ind}, and in turn to estimate L with a given precision. For example, with approximately nine samples, the proportional uncertainty (or coefficient of variation) of the standard deviation is approximately 1/4 (Figure 9), therefore with true bioturbation depths of 10 or 2 cm we would expect estimates of $10 + -2.5$ cm or $2 + -0.5$ cm respectively.

$$SE_{\sigma_{ind}} = \frac{\sigma_{ind}}{\sqrt{2(n_s - 1)}} \tag{6}$$

Finally, while the estimates of age-heterogeneity themselves remain valid, fluctuations in the abundance of the foraminifera or other signal carriers can increase or decrease age-heterogeneity such that inferred bioturbation depths are over- or under-estimated. These effects can be modeled with a number of existing tools (Dolman & Laepple, 2018; Lougheed, 2020; Trauth, 2013). The wider use of proxy forward modeling will also make clear the kind of paleoclimate questions that can and cannot be addressed using low sedimentation rate cores.

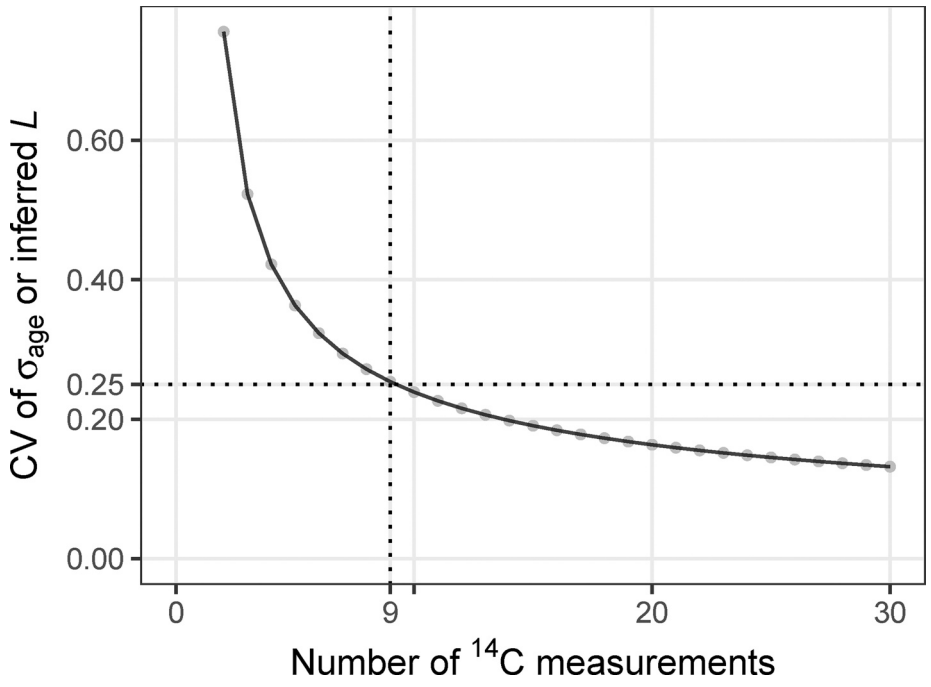

Figure 9. Coefficient of variation for estimates of σ_{age} or the implied bioturbation depth L as a function of the number of dated samples n_{rep}. Dashed lines indicate that for nine replicated ^{14}C measurements there would be a 25% uncertainty in the estimated values of σ_{age} and L.

5. Conclusions

An awareness of bioturbation and its potential influence on sedimentary proxy records due to the age-heterogeneity it causes is not new (e.g., Andree, 1987; Goreau, 1980; Keigwin & Guilderson, 2009; Schiffelbein, 1985; Steiner et al., 2016); however, it has only recently become possible to directly measure the age-heterogeneity in sediment slices of the medium that is radiocarbon dated, e.g., foraminifera. We measured age-heterogeneities that imply much deeper mixing than is typically assumed in the paleo-climate literature. At the same time, we found that between core variation in age-heterogeneity could largely be explained by sedimentation rates, which implies a relatively consistent mixed layer depth. It is conceivable that the "paleo" bioturbation depth is larger and less variable than measurements of contemporary bioturbation depths would imply (e.g., Solan et al., 2019), as integrated over time, a long period of shallow mixing would be obliterated by a subsequent period of deep mixing; where "long" is relative to the sedimentation rate. The availability of small-*n* radiocarbon dating will allow us to assess how consistent bioturbation depths really are, in addition to obtaining independent estimates of age-heterogeneity to aid our interpretation of proxy climate records.

Data Availability Statement

Radiocarbon data have been archived in Pangaea (10.1594/PANGAEA.926072., Dolman et al., 2021). The *R* code to reproduce the analyses is archived at Zenodo (10.5281/zenodo.4915811., Dolman, 2021).

References

Anderson, D. M. (2001). Attenuation of millennial-scale events by bioturbation in marine sediments. *Paleoceanography*, *16*(4), 352–357. https://doi.org/10.1029/2000PA000530

Andree, M. (1987). The impact of bioturbation on AMS 14C dates on handpicked foraminifera: A statistical model. *Radiocarbon*, *29*(2), 169–175. https://doi.org/10.1017/S0033822200056927

Ausín, B., Haghipour, N., Wacker, L., Voelker, A. H. L., Hodell, D., Magill, C., et al. (2019). Radiocarbon age offsets between two surface dwelling planktonic foraminifera species during abrupt climate events in the SW Iberian margin. *Paleoceanography and Paleoclimatology*, *34*(1), 63–78. https://doi.org/10.1029/2018PA003490

Acknowledgments
We thank the scientists and crew members on board the research vessels R/V Sonne and Ocean Researcher 1 who helped with sample retrieval, especially M. Mohtadi (all GeoB cores), F. Lamy (SO213-84-2), and C.-C. Su and A. Zuhr (OR1-1218-C2-BC). Thanks are owed to R. De Pol-Holz for help with radiocarbon measurements carried out at Keck-Carbon Cycle AMS facility, and to H. Grotheer, E. Bonk and T. Gentz who carried out the MICADAS AMS analyses. N. Behrendt and L. Kafemann assisted with sample preparation. T. Ronge is acknowledged for discussion, without implying agreement on what is written in this manuscript. This is a contribution to the SPACE ERC project; this project has received funding from the European Research Council (ERC) under the European Union's Horizon 2020 research and innovation program (grant agreement no. 716092). Additionally, this work was supported by German Federal Ministry of Education and Research (BMBF) as Research for Sustainability initiative (FONA); www.fona.de through Palmod project (FKZ: 01LP1509C). Samples from core SO213-84-2 were processed and analyzed while Sze Ling Ho was supported by the Initiative and Networking Fund of the Helmholtz Association Grant VG-NH900. I acknowledge support by the AWI Open Access Fonds of Alfred-Wegener-Institut Helmholtz-Zentrum für Polar-und Meeresforschung. Open Access funding enabled and organized by Projekt DEAL.

Bard, E., Arnold, M., Duprat, J., Moyes, J., & Duplessy, J.-C. (1987). Reconstruction of the last deglaciation: Deconvolved records of δ18O profiles, micropaleontological variations and accelerator mass spectrometric 14C dating. *Climate Dynamics*, *1*(2), 101–112. https://doi.org/10.1007/BF01054479

Bard, E., Arnold, M., Mangerud, J., Paterne, M., Labeyrie, L., Duprat, J., et al. (1994). The North Atlantic atmosphere-sea surface 14C gradient during the Younger Dryas climatic event. *Earth and Planetary Science Letters*, *126*(4), 275–287. https://doi.org/10.1016/0012-821X(94)90112-0

Bard, E., & Heaton, T. J. (2021). On the tuning of plateaus in atmospheric and oceanic ^{14}C records to derive calendar chronologies of deep-sea cores and records of ^{14}C marine reservoir age changes. *Climate of the Past Discussions*, 1–36. https://doi.org/10.5194/cp-2020-164

Barker, S., Broecker, W., Clark, E., & Hajdas, I. (2007). Radiocarbon age offsets of foraminifera resulting from differential dissolution and fragmentation within the sedimentary bioturbated zone. *Paleoceanography*, *22*(2), PA2205. https://doi.org/10.1029/2006PA001354

Berger, W. H. (1968). Planktonic Foraminifera: Selective solution and paleoclimatic interpretation. *Deep-Sea Research and Oceanographic Abstracts*, *15*(1), 31–43. https://doi.org/10.1016/0011-7471(68)90027-2

Berger, W. H., & Heath, G. R. (1968). Vertical mixing in pelagic sediments. *Journal of Marine Research*, *26*(2), 134–143

Boudreau, B. P. (1998). Mean mixed depth of sediments: The wherefore and the why. *Limnology & Oceanography*, *43*(3), 524–526. https://doi.org/10.4319/lo.1998.43.3.0524

Boyle, E. A. (1984). Sampling statistic limitations on benthic foraminifera chemical and isotopic data. *Marine Geology*, *58*(1), 213–224. https://doi.org/10.1016/0025-3227(84)90124-5

Broecker, W., & Clark, E. (2011). Radiocarbon-age differences among coexisting planktic foraminifera shells: The Barker Effect. *Paleoceanography*, *26*(2), PA2222. https://doi.org/10.1029/2011PA002116

Costa, K. M., McManus, J. F., & Anderson, R. F. (2018). Radiocarbon and stable isotope evidence for changes in sediment mixing in the North Pacific over the past 30 kyr. *Radiocarbon*, *60*(01), 113–135. https://doi.org/10.1017/RDC.2017.91

Dolman, A. M. (2021). *Earth System Diagnostics/Dolman14C_2021: Publication code*. Zenodo. https://doi.org/10.5281/zenodo.4915811

Dolman, A. M., Groeneveld, J., Mollenhauer, G., Ho, S. L., & Laepple, T. (2021). Replicated radiocarbon age measurements on foraminifera from five sediment cores. *PANGAEA*. https://doi.org/10.1594/PANGAEA.926072

Dolman, A. M., Kunz, T., Groeneveld, J., & Laepple, T. (2020). Estimating the timescale-dependent uncertainty of paleoclimate records – A spectral approach. Part II: Application and interpretation. *Climate of the Past Discussions*, 1–22. https://doi.org/10.5194/cp-2019-153

Dolman, A. M., & Laepple, T. (2018). Sedproxy: A forward model for sediment-archived climate proxies. *Climate of the Past*, *14*(12), 1851–1868. https://doi.org/10.5194/cp-14-1851-2018

Fagault, Y., Tuna, T., Rostek, F., & Bard, E. (2019). Radiocarbon dating small carbonate samples with the gas ion source of AixMICADAS. *Nuclear Instruments and Methods in Physics Research Section B: Beam Interactions with Materials and Atoms*, *455*, 276–283. https://doi.org/10.1016/j.nimb.2018.11.018

Goreau, T. J. (1980). Frequency sensitivity of the deep-sea climatic record. *Nature*, *287*(5783), 620–622. https://doi.org/10.1038/287620a0

Gottschalk, J., Szidat, S., Michel, E., Mazaud, A., Salazar, G., Battaglia, M., et al. (2018). Radiocarbon measurements of small-size foraminiferal samples with the mini carbon dating system (MICADAS) at the University of Bern: Implications for paleoclimate reconstructions. *Radiocarbon*, *60*(2), 469–491. https://doi.org/10.1017/RDC.2018.3

Groeneveld, J., Ho, S. L., Mackensen, A., Mohtadi, M., & Laepple, T. (2019). Deciphering the variability in Mg/Ca and stable oxygen isotopes of individual foraminifera. *Paleoceanography and Paleoclimatology*, *34*, 755–773. https://doi.org/10.1029/2018PA003533

Guinasso, N. L. G., & Schink, D. R. (1975). Quantitative estimates of biological mixing rates in abyssal sediments. *Journal of Geophysical Research*, *80*(21), 3032–3043. https://doi.org/10.1029/JC080i021p03032

Haslett, J., & Parnell, A. (2008). A simple monotone process with application to radiocarbon-dated depth chronologies. *Journal of the Royal Statistical Society: Series C (Applied Statistics)*, *57*(4), 399–418. https://doi.org/10.1111/j.1467-9876.2008.00623.x

Heaton, T. J., Köhler, P., Butzin, M., Bard, E., Reimer, R. W., Austin, W. E. N., et al. (2020). Marine20—The marine radiocarbon age calibration curve (0–55,000 cal BP). *Radiocarbon*, *62*(4), 779–820. https://doi.org/10.1017/RDC.2020.68

Hebbeln, D., & cruise participants. (2006). *Report and preliminary results of RV Sonne Cruise SO-184, Pabesia, Durban (South Africa) - Cilacap (Indonesia) - Darwin (Australia) July 8th - September 13th, 2005*. Department of Geosciences, Bremen University. *246*.

Heegaard, E., Birks, H. J. B., & Telford, R. J. (2005). Relationships between calibrated ages and depth in stratigraphical sequences: An estimation procedure by mixed-effect regression. *The Holocene*, *15*(4), 612–618. https://doi.org/10.1191/0959683605hl836rr

Keigwin, L. D., & Guilderson, T. P. (2009). Bioturbation artifacts in zero-age sediments. *Paleoceanography*, *24*(4), PA4212. https://doi.org/10.1029/2008PA001727

Key, R. (2001). Radiocarbon. In *Encyclopedia of ocean sciences* (pp. 2338–2353). Elsevier. https://doi.org/10.1006/rwos.2001.0162

Koutavas, A., & Joanides, S. (2012). El Niño–Southern oscillation extrema in the Holocene and last glacial maximum. *Paleoceanography*, *27*(4), PA4208. https://doi.org/10.1029/2012PA002378

Kunz, T., Dolman, A. M., & Laepple, T. (2020). A spectral approach to estimating the timescale-dependent uncertainty of paleoclimate records – Part 1: Theoretical concept. *Climate of the Past*, *16*(4), 1469–1492. https://doi.org/10.5194/cp-16-1469-2020

Küssner, K., Sarnthein, M., Lamy, F., & Tiedemann, R. (2018). High-resolution radiocarbon records trace episodes of Zoophycos burrowing. *Marine Geology*, *403*, 48–56. https://doi.org/10.1016/j.margeo.2018.04.013

Lea, D. W. (2014). Elemental and isotopic proxies of past ocean temperatures. *Treatise on Geochemistr* (2nd ed., 1–16, pp. 373–397). Elsevier. https://doi.org/10.1016/b978-0-08-095975-7.00614-8

Lougheed, B. C. (2020). SEAMUS (v1.20): A Δ^{14}C-enabled, single-specimen sediment accumulation simulator. *Geoscientific Model Development*, *13*(1), 155–168. https://doi.org/10.5194/gmd-13-155-2020

Lougheed, B. C., Ascough, P., Dolman, A. M., Löwemark, L., & Metcalfe, B. (2020). Re-evaluating ^{14}C dating accuracy in deep-sea sediment archives. *Geochronology*, *2*(1), 17–31. https://doi.org/10.5194/gchron-2-17-2020

Lougheed, B. C., Metcalfe, B., Ninnemann, U. S., & Wacker, L. (2018). Moving beyond the age–depth model paradigm in deep-sea palaeoclimate archives: Dual radiocarbon and stable isotope analysis on single foraminifera. *Climate of the Past*, *14*(4), 515–526. https://doi.org/10.5194/cp-14-515-2018

Lougheed, B. C., Snowball, I., Moros, M., Kabel, K., Muscheler, R., Virtasalo, J. J., & Wacker, L. (2012). Using an independent geochronology based on palaeomagnetic secular variation (PSV) and atmospheric Pb deposition to date Baltic Sea sediments and infer 14C reservoir age. *Quaternary Science Reviews*, *42*, 43–58. https://doi.org/10.1016/j.quascirev.2012.03.013

Löwemark, L., & Grootes, P. M. (2004). Large age differences between planktic foraminifers caused by abundance variations and Zoophycos bioturbation. *Paleoceanography*, *19*(2), PA2001. https://doi.org/10.1029/2003PA000949

Löwemark, L., Konstantinou, K., & Steinke, S. (2008). Bias in foraminiferal multispecies reconstructions of paleohydrographic conditions caused by foraminiferal abundance variations and bioturbational mixing: A model approach. *Marine Geology*, *256*(1–4), 101–106. https://doi.org/10.1016/j.margeo.2008.10.005

Löwemark, L., & Werner, F. (2001). Dating errors in high-resolution stratigraphy: A detailed X-ray radiograph and AMS-14C study of Zoophycos burrows. *Marine Geology*, *177*(3), 191–198. https://doi.org/10.1016/S0025-3227(01)00167-0

Matisoff, G. (1982). Mathematical models of bioturbation. In P. L. McCall, & M. J. S. Tevesz (Eds.), *Animal-sediment relations: The biogenic alteration of sediments* (pp. 289–330). Springer. https://doi.org/10.1007/978-1-4757-1317-6_7

Mollenhauer, G., Grotheer, H., Gentz, T., Bonk, E., & Hefter, J. (2021). Standard operation procedures and performance of the MICADAS radiocarbon laboratory at Alfred Wegener Institute (AWI), Germany. *Nuclear Instruments and Methods in Physics Research Section B: Beam Interactions with Materials and Atoms*, *496*, 45–51. https://doi.org/10.1016/j.nimb.2021.03.016

Nürnberg, D., Bijma, J., & Hemleben, C. (1996). Assessing the reliability of magnesium in foraminiferal calcite as a proxy for water mass temperatures. *Geochimica et Cosmochimica Acta*, *60*(5), 803–814. https://doi.org/10.1016/0016-7037(95)00446-7

Officer, C., & Lynch, D. (1983). Determination of mixing parameters from tracer distributions in deep-sea sediment cores. *Marine Geology*, *52*(1–2), 59–74. https://doi.org/10.1016/0025-3227(83)90021-X

Peng, T.-H., & Broecker, W. S. (1984). The impacts of bioturbation on the age difference between benthic and planktonic foraminifera in deep sea sediments. *Nuclear Instruments and Methods in Physics Research Section B: Beam Interactions with Materials and Atoms*, *5*(2), 346–352. https://doi.org/10.1016/0168-583X(84)90540-8

R Core Team. (2019). *R: A language and environment for statistical computing*.

Rosenthal, Y., Lohmann, G. P., Lohmann, K. C., & Sherrell, R. M. (2000). Incorporation and preservation of Mg in Globigerinoides sacculifer: Implications for reconstructing the temperature and 18O/16O of seawater. *Paleoceanography*, *15*(1), 135–145. https://doi.org/10.1029/1999PA000415

Ruff, M., Szidat, S., Gäggeler, H. W., Suter, M., Synal, H. A., & Wacker, L. (2010). Gaseous radiocarbon measurements of small samples. *Nuclear Instruments and Methods in Physics Research Section B: Beam Interactions with Materials and Atoms*, *268*(7), 790–794. https://doi.org/10.1016/j.nimb.2009.10.032

Schiffelbein, P. (1985). Calculation of error measures for deconvolved deep-sea stratigraphic records. *Marine Geology*, *65*(3), 333–342. https://doi.org/10.1016/0025-3227(85)90063-5

Schiffelbein, P., & Hills, S. (1984). Direct assessment of stable isotope variability in planktonic foraminifera populations. *Palaeogeography, Palaeoclimatology, Palaeoecology*, *48*(2), 197–213. https://doi.org/10.1016/0031-0182(84)90044-0

Solan, M., Ward, E. R., White, E. L., Hibberd, E. E., Cassidy, C., Schuster, J. M., et al. (2019). Worldwide measurements of bioturbation intensity, ventilation rate, and the mixing depth of marine sediments. *Scientific Data*, *6*(1), 58. https://doi.org/10.1038/s41597-019-0069-7

Steiner, Z., Lazar, B., Levi, S., Tsroya, S., Pelled, O., Bookman, R., & Erez, J. (2016). The effect of bioturbation in pelagic sediments: Lessons from radioactive tracers and planktonic foraminifera in the Gulf of Aqaba, Red Sea. *Geochimica et Cosmochimica Acta*, *194*, 139–152. https://doi.org/10.1016/j.gca.2016.08.037

Sun, S., Meyer, V. D., Dolman, A. M., Winterfeld, M., Hefter, J., Dummann, W., et al. (2020). 14C blank assessment in small-scale compound-specific radiocarbon analysis of lipid biomarkers and lignin phenols. *Radiocarbon*, *62*(1), 207–218. https://doi.org/10.1017/RDC.2019.108

Teal, L., Bulling, M., Parker, E., & Solan, M. (2010). Global patterns of bioturbation intensity and mixed depth of marine soft sediments. *Aquatic Biology*, *2*(3), 207–218. https://doi.org/10.3354/ab00052

Thirumalai, K., DiNezio, P. N., Tierney, J. E., Puy, M., & Mohtadi, M. (2019). An El Niño mode in the Glacial Indian Ocean? *Paleoceanography and Paleoclimatology*, *34*, 1316–1327. https://doi.org/10.1029/2019PA003669

Thirumalai, K., Partin, J. W., Jackson, C. S., & Quinn, T. M. (2013). Statistical constraints on El Niño Southern Oscillation reconstructions using individual foraminifera: A sensitivity analysis. *Paleoceanography*, *28*(3), 401–412. https://doi.org/10.1002/palo.20037

Thomson, J., Cook, G. T., Anderson, R., MacKenzie, A. B., Harkness, D. D., & McCave, I. N. (1995). Radiocarbon age offsets in different-sized carbonate components of deep-sea sediments. *Radiocarbon*, *37*(2), 91–101. https://doi.org/10.1017/S0033822200030526

Thornalley, D. J. R., McCave, I. N., & Elderfield, H. (2010). Freshwater input and abrupt deglacial climate change in the North Atlantic. *Paleoceanography*, *25*(1), PA1201. https://doi.org/10.1029/2009PA001772

Tiedemann, R., Lamy, F., Molina-Kescher, M., Tapia Arroyo, R., Poggemann, D. W., & Nürnberg, D. (2014). *FS Sonne Fahrtbericht / Cruise Report SO213 - SOPATRA: South Pacific Paleoceanographic Transects - Geodynamic and Climatic Variability in Space and Time, Leg 1: Valparaiso/Chile - Valparaiso/Chile, 27.12.2010 - 12.01.2011 and Leg 2: Valparaiso/Chile - Wellington/New Zealand, 12.01.2011 - 07.03.2011 (Report)*. https://doi.org/10.2312/crso213

Trauth, M. H. (2013). TURBO2. *Computers & Geosciences*, *61*(C), 1–10. https://doi.org/10.1016/j.cageo.2013.05.003

Trauth, M. H., Sarnthein, M., & Arnold, M. (1997). Bioturbational mixing depth and carbon flux at the seafloor. *Paleoceanography*, *12*(3), 517–526. https://doi.org/10.1029/97PA00722

Wacker, L., Bonani, G., Friedrich, M., Hajdas, I., Kromer, B., Nemec, N., et al. (2010). MICADAS: Routine and high-precision radiocarbon dating. *Radiocarbon*, *52*(2), 252–262. https://doi.org/10.1017/S0033822200045288

Wacker, L., Lippold, J., Molnár, M., & Schulz, H. (2013). Towards radiocarbon dating of single foraminifera with a gas ion source. *Nuclear Instruments and Methods in Physics Research Section B: Beam Interactions with Materials and Atoms*, *294*, 307–310. https://doi.org/10.1016/j.nimb.2012.08.038

Wetzel, A., & Werner, F. (1980). Morphology and ecological significance of Zoophycos in deep-sea sediments off NW Africa. *Palaeogeography, Palaeoclimatology, Palaeoecology*, *32*, 185–212. https://doi.org/10.1016/0031-0182(80)90040-1

Wheatcroft, R. A. (1992). Experimental tests for particle size-dependent bioturbation in the deep ocean. *Limnology & Oceanography*, *37*(1), 90–104. https://doi.org/10.4319/lo.1992.37.1.0090

Wit, J., Reichart, G., & Ganssen, G. (2013). Unmixing of stable isotope signals using single specimen δ18O analyses. *Geochemistry, Geophysics, Geosystems*, *14*(4), 1312–1320. https://doi.org/10.1002/ggge.20101